TITLE:

Relationship Between Permeability and Resistivity of Sheared Rock Fractures: The Role of Tortuosity and Flow Path Percolation

AUTHOR(S):

Sawayama, K.; Ishibashi, T.; Jiang, F.; Tsuji, T.

京都大学
KYOTO UNIVERSITY

KURENAI 紅
Kyoto University Research Information Repository

AGU
ADVANCING EARTH AND SPACE SCIENCES

Geophysical Research Letters®

Key Points:

- Numerical results clarify the dependencies of fracture size, roughness, shear displacement, and stress on permeability and resistivity
- Flow path percolation can be correlated with tortuosity, which controls the rigorous resistivity–porosity and –permeability relationships
- Archie's exponent is constant for a percolated single fracture and can be used for monitoring permeability and pore pressure change

Author Contributions:

Conceptualization: K. Sawayama
Data curation: K. Sawayama
Formal analysis: K. Sawayama
Funding acquisition: K. Sawayama, T. Tsuji
Investigation: K. Sawayama
Methodology: K. Sawayama
Resources: K. Sawayama
Software: K. Sawayama, F. Jiang
Validation: K. Sawayama
Visualization: K. Sawayama
Writing – original draft: K. Sawayama
Writing – review & editing: T. Ishibashi, F. Jiang, T. Tsuji

Relationship Between Permeability and Resistivity of Sheared Rock Fractures: The Role of Tortuosity and Flow Path Percolation

K. Sawayama[1] , T. Ishibashi[2] , F. Jiang[3], and T. Tsuji[4]

[1]Institute for Geothermal Sciences, Graduate School of Science, Kyoto University, Beppu, Japan, [2]Fukushima Renewable Energy Institute, National Institute of Advanced Industrial Science and Technology, Koriyama, Japan, [3]Department of Mechanical Engineering, Graduate School of Sciences and Technology for Innovation, Yamaguchi University, Ube, Japan, [4]School of Engineering, The University of Tokyo, Tokyo, Japan

Abstract The fluid-flow properties of fractures have received increasing attention regarding the role of geofluids in the genesis of slow and fast earthquakes and recent advances in geoengineering developments. Geophysical observations are promising tools to remotely estimate crustal permeability changes; however, quantitative interpretations are limited by the rock-physical models' paucity for fractures. This study investigated changes in permeability, resistivity, and their respective relationships at elevated stress by performing numerical simulations of different fracture models with varying fracture size, roughness, and shear displacement. Numerical results and microscopic flow analysis demonstrate that permeability–resistivity relationships are controlled by percolation and are less dependent on fracture geometric characteristics. Our finding suggests that the permeability evolution of fractures can be formulated with resistivity changes independent of both fracture size and microstructure, the trends of which can be predicted using Archie's exponent. The extension to the electro-mechanical relationship further derives the potential applications of estimating stress changes.

Plain Language Summary Monitoring the flow of fluids through underground fractures is important for developing earth resources and understanding the generation of both slow and fast earthquakes. This can be realized by observing physical properties underground such as electrical resistivity; however, the relationships between electrical and hydraulic properties are poorly understood because we have limited data on rock fractures. Thus, in this study, we explored changes in the hydraulic and electrical properties of synthetic rock fractures by subjecting them to increasing normal stress and shear displacement while varying the properties of the fracture surface topographies and length scales referring to natural data. We formulated the relationship between electrical resistivity and permeability invariant of fracture size, roughness, shear displacement, and normal stress based on both the theoretical model and empirical Archie's equation. We found that the rigorous relationship is controlled by the local connection of the fluid-flow paths based on the microscopic flow analysis. The proposed formula can estimate the permeability evolution of fractures using resistivity data and is a better approach compared to porosity estimation because resistivity–porosity relationship can change depending on the tortuosity or connectivity. The extension to the electro-mechanical relationship also derives the potential applications of estimating changes in pore pressure.

1. Introduction

The fluid-flow characteristics of fractured geological formations are of critical interest in a number of areas, including the assessment of seismic hazards (slow slip, fault reactivation, and induced seismicity), fluid resources (e.g., geothermal fluids, shale oil, and groundwater), and geological storage or disposal. Numerous studies have demonstrated that fluid-flow properties are constrained by heterogeneous aperture distribution of the fracture (Chen et al., 2017; Witherspoon et al., 1980; Zimmerman et al., 1992), which can be altered by shear displacement and stress (Durham & Bonner, 1994; Ishibashi et al., 2015; Pyrak-Nolte & Morris, 2000; Tsang & Witherspoon, 1981; Vogler et al., 2018; R. Walsh et al., 2008; Watanabe et al., 2008). Recent studies have identified that seismically induced permeability changes in both field observations (Elkhoury et al., 2006; Y. Shi et al., 2019; Z. Shi et al., 2018; Sun et al., 2019) and laboratory experiments (Candela et al., 2014, 2015; Elkhoury et al., 2011; Elsworth et al., 2018; Shokouhi et al., 2020; Wood et al., 2021) are caused by transient changes in

stress and the shear displacement of faults. Given that in situ stresses are never constant throughout geoengineering developments or on the geological time scale, these impacts must be considerable in natural settings even in the absence of major seismicity.

Although direct measurement of permeability changes is a challenging task, geophysical observation using electrical resistivity is a potential approach. In a wide range of fields, electromagnetic surveys have observed resistivity changes that are associated with subsurface stress changes, such as geothermal activity, fluid production, and seismicity (Aizawa et al., 2011; Didana et al., 2017; Johnson et al., 2021; Mazzella & Morrison, 1974; Park, 1991; Peacock et al., 2012, 2013). It would be advantageous if changes in permeability caused by variations in the subsurface stress could be linked to electrical resistivity, which could be monitored remotely. Several models have been proposed on the relation between permeability and resistivity of porous media (Bernabé et al., 2011; Cai et al., 2019; Ghanbarian & Male, 2021; Glover et al., 2006; Hilfer, 1992; Katz & Thompson, 1986; Revil & Cathles, 1999). Such models allow the estimation of permeability from resistivity data (Anderson et al., 1985; Becker et al., 1982; Katayama et al., 2020; Slagle & Goldberg, 2011; Yamaya et al., 2022). However, some field observations have detected unusual changes in permeability and resistivity (Park, 1991; Xue et al., 2013) that could not be explained by experimental findings due to the existence of a macroscopic fracture in the fields. More recent observations also evoke the importance of macroscopic fractures as they contribute to the anomalously high permeability in the underthrust, which may be related to the pore pressure supply and the generation of slow earthquakes (Heuler et al., 2017; Hirose et al., 2021). However, the paucity of data using fractured rock mass hinders attempts at updating the rock-physical models that can be used to evaluate changes in permeability. A pioneering study by Stesky (1986) reported that permeability and resistivity in saw-cut fractures are linearly related in a logarithmic coordinate. Conversely, numerical studies based on rough-walled fractures have reported a nonlinear relationship resulting from the heterogeneous flow distributions (Kirkby et al., 2016; Sawayama et al., 2021a), similar to the previously reported percolation for fracture permeability (Berkowitz, 1995; Pyrak-Nolte et al., 1988). However, how the fracture geometric characteristics affect the percolation and its impact on the permeability–resistivity relationship remains unclear.

Thus, this study employed a digital rock physics approach (Andrä et al., 2013; Sawayama et al., 2022) to determine permeability and resistivity simultaneously while assessing the evolution in local connections and percolation of preferential flow paths with the elevated normal stress and shear displacement. We discuss the role of local flow behavior on permeability, resistivity, and their respective relationships, and suggest potential practical applications of our findings.

2. Methodology

We conducted a series of numerical simulations of fluid flow and electrical conduction within deformed rock fractures. The fracture surface topography is known to be self-affine fractal and can be created numerically (Brown, 1995; Matsuki et al., 2006). Following these studies, synthetic fracture models with controlled roughness and shear displacement were generated based on the fractional Brownian motion (Text S1 in Supporting Information S1). To investigate the effect of the fractal characteristics, the fractal dimension D and surface roughness s (i.e., the root mean square height of the surface topography) were varied as $D = 2.0, 2.2, 2.4$ and $s = 0.1, 0.2, 0.3$ mm referring to natural faults (Brown & Scholz, 1985; Power & Durham, 1997; Power et al., 1987). Note that such fractal nature has been confirmed as valid for natural fault roughness from local to global scales (Candela & Brodsky, 2016; Candela et al., 2012; Renard & Candela, 2013). Based on these values, we prepared a synthetic fracture model of varying fracture size $L = 24, 48, 96$ mm with a 0.1-mm square grid, where a well-known scaling law for fracture roughness was incorporated (Matsuki et al., 2006):

$$s = s_0 \left(\frac{L}{L_0} \right)^{3-D}. \tag{1}$$

Here, the subscript zero represents the reference model ($L_0 = 24$ mm, $s_0 = 0.1, 0.2, 0.3$ mm). For each fracture model, we numerically simulated the elastic-fully plastic deformation of the asperities using a half space–based dry contact model with up to 100 MPa of normal loading (Polonsky & Keer, 1999). The corresponding algorithm is summarized in Text S2 in Supporting Information S1. The boundary was treated as periodic to eliminate the boundary effect (Petrovitch et al., 2014). We confirmed that the constructed aperture, that is, the gap of the deformed rough surface, follows the scaling law (Figure S2 in Supporting Information S1) observed

in natural joints and faults (Kim & Sanderson, 2005; Schlische et al., 1996; Schultz et al., 2008). The variations in mean aperture value and the aperture distribution against stress are shown in Figure S3 in Supporting Information S1. Furthermore, additional 13,000 simulations (for a total of 14,530) were performed by varying the random seeds to investigate the stochastic fluctuations of our simulation results (Text S1 in Supporting Information S1).

We then simulated 3D fracture flows using the lattice Boltzmann method, where we adopted a multi-relaxation-time D3Q19 model (Ahrenholz et al., 2008; Jiang et al., 2014; Sawayama et al., 2021a). The provision of a constant body force from the inlet to the outlet boundaries and the periodic boundary along the fracture plane allowed us to simulate the fracture flows in the directions perpendicular to the shear direction (Figure S4 in Supporting Information S1). Then, the fracture permeability was estimated from the macroscopic flow velocity, assuming Darcy flow and negligible matrix permeability ($\sim 10^{-20}$ m^2). Subsequently, we analyzed resistivity using the finite element method (Garboczi, 1998; Sawayama et al., 2021b). Similar to the fluid flow, we simulated the local field of electric currents in the direction perpendicular to the shear direction, and calculated corresponding resistivity. In this analysis, fluid and solid conductivities of 5 and 10^{-5} S/m, respectively, were modeled (Sawayama et al., 2018). We also evaluated the bulk permeability and resistivity of the fractured rock mass having a constant thickness ($n_z = 24$ mm) to consider the porosity effect. This enables us to correlate the permeability–resistivity relationship within the same elementary volume. Notably, the relationship does not change regardless of the thickness value even though their absolute values change, when matrix permeability and resistivity are presumed to be negligible. Then, we calculated the formation factor F by dividing the bulk resistivity ρ_b by the fluid resistivity ρ_w, ($F = \rho_b/\rho_w$) such that the effects of both the temperature and salinity on fluid resistivity can be neglected.

3. Results and Discussion

3.1. Changes in Permeability and Resistivity as Elevated Normal Stress

We present the evolution of permeability, electrical resistivity, and the associated changes of the local flow paths of various fracture data sets as elevated normal stress (Figure 1). The results demonstrate the dependencies of fracture size (Figures 1a and 1b), shear displacement ratio (Figures 1c and 1d), and surface roughness characteristics (Figures 1e and 1f) on these properties. Permeability and resistivity of joints (i.e., no shear displacement) are less dependent on fracture size, as previous studies have reported (Ishibashi et al., 2015; Sawayama et al., 2021b). In addition, faults (i.e., sheared fractures) exhibit scale-dependent characteristics, where permeability increases and resistivity decreases remarkably with fracture size (Figures 1a and 1b). The stress-dependent changes in permeability and resistivity are significant in fractures with larger shear displacements (Figures 1c and 1d). The roughness increases permeability and decreases resistivity, and these properties are nearly constant under different fractal dimensions (Figures 1e and 1f). The higher roughness of the fracture surfaces (i.e., rms height s) increases the aperture because it enhances the mismatch between two surfaces, and thus leads to higher permeability and lower resistivity (Figure S5 in Supporting Information S1). The roughness effect will change depending on the shear displacement (Figure S5 in Supporting Information S1) and the two orthogonal directions (Figure S6 in Supporting Information S1). The effects of shear displacement and roughness become insignificant under higher stress conditions (Figures 1c–1f).

The panels at the bottom of Figure 1 show representative simulation results for the evolutions of fracture flow within the heterogeneous aperture distribution with and without shear displacement. Note that the flow rates have been vertically summed in every z-direction and the regions with >1% of the maximum is visualized such that the dominant paths in the fractures can be projected onto the x–y plane. At the lowest stresses, dominant flow paths induce channeling that covers most of the open space (Figure 1, images i and iv). As the stress increases, larger portions of the fracture surfaces are in contact; thus, the channeling paths decrease progressively and become narrow (Figure 1, images ii and v). Further normal loading diminishes the dominant flow paths. Accordingly, the flow paths from the inlet to the outlet lose their connection (Figure 1, images iii and vi). This phenomenon is nearly the same in both joints and faults. The stress level at which this transition occurs can be defined as the percolation threshold that considerably controls the transport behaviors of rocks (Berkowitz, 1995; Ghanbarian et al., 2014; Guéguen et al., 1997; Pyrak-Nolte et al., 1988). Above this percolation threshold, permeability, and resistivity demonstrate different trends against changes in stress.
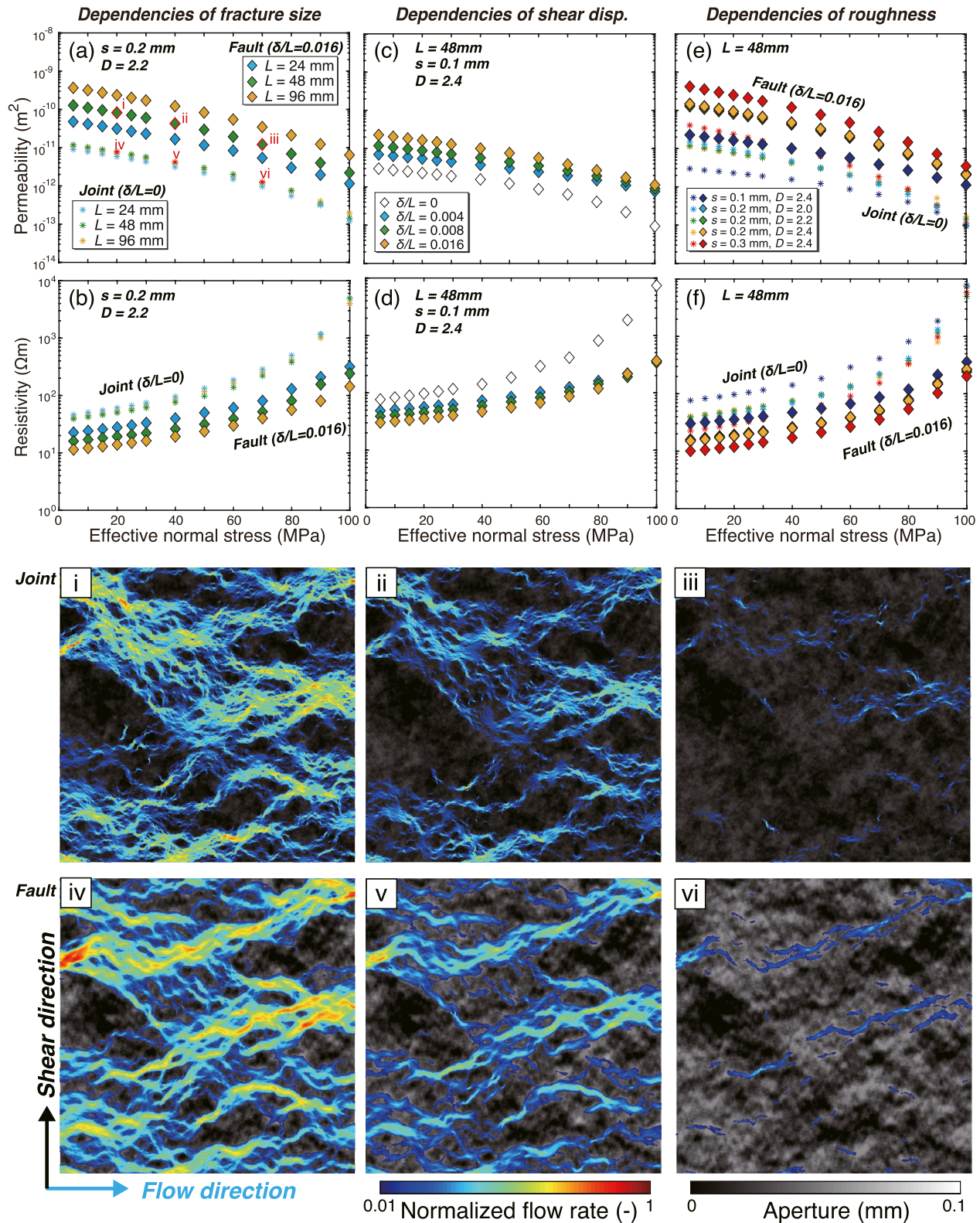
Figure 1. Plots of permeability and resistivity changes as a function of normal stress (a–f) and representative images derived from the simulation showing the local flow distributions (color) overlaid on the aperture distributions (grayscale) for (i–iii) joints and (iv–vi) faults. The stress levels of images (i–vi) are shown in panel (a). L, δ, s, and D represent the fracture length, shear displacement, roughness, and fractal dimension, respectively.
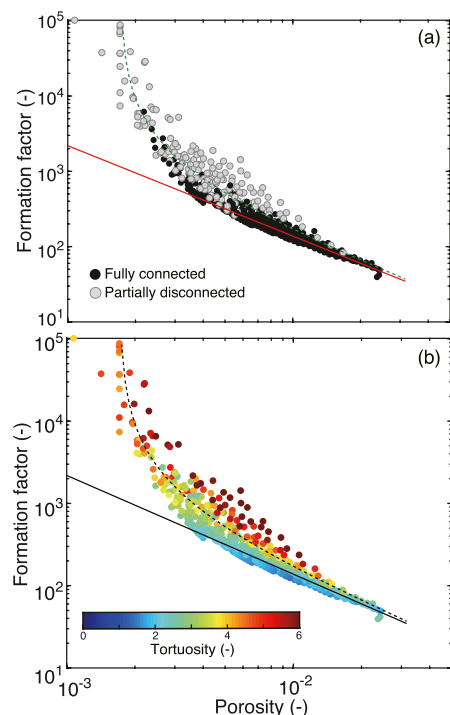
Figure 2. Correlations between formation factor and porosity with respect to (a) flow path percolation and (b) tortuosity. Note that the formation factor indicates bulk resistivity normalized by fluid resistivity. The solid and dashed lines are approximation lines based on Equation 2 ($m = 1.2$) and Equation 3 considering a percolation porosity of 0.17%, respectively.

3.2. Effect of Percolation and Tortuosity on Resistivity

It is known that resistivity has a power law relationship with porosity (Archie, 1942):

$$F = \rho_b / \rho_w = a\varphi^{-m}, \tag{2}$$

where φ is porosity, and a and m are empirical coefficients. Previous studies pointed out that m, the so-called cementation exponent, is dependent on pore connectivity (Glover, 2009; Guéguen & Palciauskas, 1994). Based on the local fluid paths (Figure 1, images i–vi) in each condition, we examine whether the dominant flow paths (i.e., >1% of the maximum flow rate; Figure 1) are fully connected throughout the model using the image processing technique (i.e., bounding box). Consequently, we have classified all results into fully connected and partially disconnected flow regimes of the dominant paths (Figure S7 in Supporting Information S1). Figure 2a plots the formation factor and porosity relative to these flow regimes. Overall, our results in the fully connected flow regime demonstrate a linear trend in the log–log plot (Figure 2a), which is consistent with Archie's exponent $m = 1.2$. Conversely, the results of the partially disconnected flow regime deviated from the linear line. This nonArchie behavior suggests that the connectivity of the dominant flow path was lost at this state. Note that the threshold value varied slightly (but not significantly) with different fracture geometric characteristics (i.e., the fracture size, shear displacement, and surface roughness characteristics). By introducing such percolation porosity, that is, φ_p, Equation 2 can also be expressed as follows:

$$F = a(\varphi - \varphi_p)^{-m}. \tag{3}$$

The percolation porosity obtained via curve fitting of all the results was 0.17% (dashed lines in Figure 2), which is greater than granular materials (~1%–3%, Colombier et al., 2017; Revil et al., 2014) because most of the pore spaces contributed to the flow in our fracture case relative to the porous media. Given such a small porosity in a fractured rock mass (average of 0.8% in our case), the low percolation porosity value is considered reasonable (Hunt & Sahimi, 2017).

Below this percolation threshold, the formation factor was not constant even for similar porosity data, which may reflect the different connectivity (Gueguen & Dienes, 1989), although quantitative analysis of the connectivity is difficult after disconnection of the dominant flow paths. Thus, we evaluated the tortuosity τ^2 of the flow paths because this is comparable to the connectivity c as the following relation (Text S3 in Supporting Information S1):

$$\tau^2 = \frac{5}{2c} \tag{4}$$

This relation demonstrates that the tortuosity should be equal to or less than 2.5 while the flow path is connected ($c = 1$). Figure 2b shows the effect of tortuosity on Archie's relation. Notably, the data sets of $\tau^2 \leq 2.5$ are consistent with the linear line ($m = 1.2$), representing the fully connected flow regime (the red line in Figure 2a). Above this threshold value, the tortuosity enhances the formation factor even when the fractures have the same porosity, thereby exhibiting nonArchie behavior (i.e., the resistivity deviates from the linear line). Higher tortuosity corresponds to a longer current path (Text S3 in Supporting Information S1), thereby enhancing the formation factor. These results clarify the role of tortuosity on resistivity. Additionally, such a percolation trend also affects the permeability–resistivity relationship, which is discussed in the following section.

3.3. Relationship Between Permeability and Resistivity

Despite of the dependencies of fracture size, shear displacement and surface roughness characteristics on permeability and resistivity (Figure 1), we found that their respective correlations exhibit stable trends invariant of these characteristics (Figure 3). The relationship between permeability k and the formation factor (hereafter referred to as the k–F relationship) can be correlated as follows with two different slopes α.
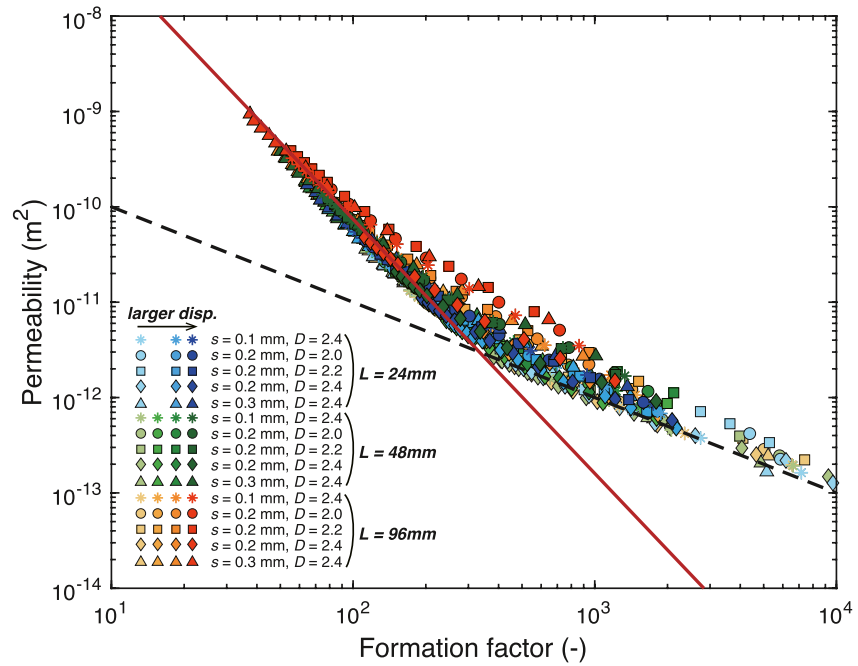
Geophysical Research Letters

Figure 3. Correlation between formation factor and permeability compiled for all fracture data sets. The symbols' color and shape represent different fracture length scales, shear displacement, roughness, and fractal dimension values. The solid and dashed lines denote prediction lines based on Equation 5 for $\alpha = 2.7$ and $\alpha = 1.0$, respectively.

$$k \propto F^{-\alpha} \tag{5}$$

Overall, the slope α remains constant regardless of the different fracture geometric characteristics. Based on the equivalent channel model, changes in bulk permeability and formation factor at elevated stress can be interpreted theoretically as changes in tortuosity and aperture d (Paterson, 1983; Sawayama et al., 2021b; J. B. Walsh & Brace, 1984).

$$k = \frac{d^2 \varphi}{12 \tau^2} \tag{6}$$

$$F = \frac{\tau^2}{\varphi} \tag{7}$$

Focusing on the changes in permeability and formation factor from the arbitrary references (i.e., k_o and F_o) such as monitoring purposes, Equation 5 can be written as follows:

$$\frac{k}{k_o} = \frac{F}{F_o}^{-\alpha} \tag{8}$$

Substituting Equation 6 and Equation 7 into Equation 8 derives the following (the detailed derivation is described in Sawayama et al. (2021b):

$$\log \frac{\tau^2}{\tau_o^2} = \frac{3 - \alpha}{1 - \alpha} \log \frac{d}{d_o}, \tag{9}$$

where the subscript zero indicates an arbitrary reference value. This demonstrates that the slope α represents the sensitivity of the tortuosity against aperture closure and is bounded between values of 1 and 3. To this point, the inflection of the k–F relationship (at $k = \sim 10^{-11.5}$) may represent the transition of their different sensitivities to tortuosity under fully connected and partially disconnected flow regimes, that is, the effect of percolation because of the channeling of the limited flow paths. Our results (Figure 3) for higher permeability (i.e., the fully connected flow regime) are plotted on the straight line of $\alpha = 2.7$ (close to 3), which indicates that the change in tortuosity

京都大学
KYOTO UNIVERSITY

A Self-archived copy in
Kyoto University Research Information Repository
https://repository.kulib.kyoto-u.ac.jp

京都大学学術情報リポジトリ
KURENAI 紅
Kyoto University Research Information Repository

AGU
ADVANCING EARTH
AND SPACE SCIENCES

Geophysical Research Letters

10.1029/2023GL104418

is very sensitive to aperture change. As shown in Figure 3, the fully connected flow regime is consistent with Archie's relation. Given the similarity of Equation 2 and Equation 7, we can derive the following relation (Text S4 in Supporting Information S1):

$$\alpha = \frac{2+m}{m}.$$

(10)

Substituting $m = 1.2$ into Equation 10 leads to $\alpha = 2.7$. Meanwhile, our results show $\alpha = 1.0$ below the percolation threshold (i.e., the partially disconnected flow regime). This is the lower limit expected based on the equivalent channel model (Equation 9), which indicates that the change in tortuosity is insensitive to aperture closure (Brown, 1989). In both cases, our findings could suggest that the permeability change can be estimated without knowing the absolute value of the permeability but with the observed resistivity data and the slope α, which can be derived from Archie's exponent (Equation 10) in the fully connected flow regime or is unity in the partially disconnected flow regime. Notably, additional 13,000 simulations with varying random seeds validated the rigidity of the proposed relationship at our simulation scale (Figure S8 in Supporting Information S1).

4. Implications

We have presented how permeability, resistivity, and porosity are affected by fracture closures and their geometrical features. In the field, by assuming a constant Archie's exponent, resistivity data are frequently interpreted as porosity (Becker et al., 1982; Chesley et al., 2021; Naif et al., 2016). We have clarified that the resistivity–porosity relationship can change depending on the tortuosity or connectivity, which indicates that we must consider Archie's exponent depending on the local connection of the flow paths. This is particularly important when a macroscopic fracture is present. In contrast, the permeability–resistivity relationship is irrelevant to tortuosity and depends on only percolation. These findings suggest that, compared to porosity, the resistivity observation is less biased in the estimation of fracture permeability.

The presence and reactivation of mesoscale fractures and the associated changes in permeability are important for developing enhanced geothermal systems (EGS). In practice, resistivity observations in EGS projects detect resistivity changes (approximately a few percent) (Didana et al., 2017; Johnson et al., 2021; Peacock et al., 2013) that are associated with the hydraulic stimulation of preexisting fault systems. Under the assumption that α takes a value between 1 and 3 in Equation 5, these resistivity changes correspond to a few to several tens of percent increases in permeability. Note that the variability of α is entirely due to the percolation and is independent of fracture size, shear offset, fractal dimension, and fracture roughness. Below the percolation threshold (i.e., the partially disconnected regime), $\alpha = 1$ indicates that tortuosity change is nearly constant under normal stress (i.e., an aperture opening/closure). The impermeable faults may correspond to this regime, where the significance of the stagnant flow area may accelerate the mineral precipitation (Sibson, 1987) or short-circuited flow paths (Hawkins et al., 2018; Okoroafor et al., 2022) (Figure 1, images iii and vi). After the percolation, that is, the fully connected regime, a greater α value indicates that tortuosity has decayed significantly and fallen to 2.5, thereby representing connectivity of $c = 1$ (Equation 4). Above this threshold, permeability hopefully is enhanced by approximately 2.7 orders in the same resistivity change. Although estimating the percolation transition is particularly important for practical use in the field, Kirkby et al. (2016) have argued that the percolation threshold is independent of matrix permeability but dependent on the matrix-to-fluid resistivity ratio (in our case, 5×10^5) and fracture spacing. Note that our model assumes simple single fractures; thus, the changes in transport properties in intersecting fracture networks (Kirkby & Heinson, 2017; Wu et al., 2021) should be investigated further.

The success of linking the k–F relationship may be further discussed with the mechanical properties as the hydromechanical relationship is theoretically formulated (Pyrak-Nolte & Nolte, 2016; Wang & Cardenas, 2016). Hence, we attempted to incorporate the mechanical property into the resistivity model to further expand the applications. Provided the negligible matrix porosity and constant thickness of the fractured rock mass, the change in porosity of a single fracture is comparable to the aperture change. The stress-induced aperture change (i.e., displacement) can be given by the effective normal stress σ divided by the fracture specific stiffness κ, and thereby Equation 2 can be rewritten as follows:

$$\frac{F}{F_0} = \left(\frac{\varphi}{\varphi_0}\right)^{-m} = \left(\frac{d_0 - \sigma/\kappa}{d_0}\right)^{-m},$$
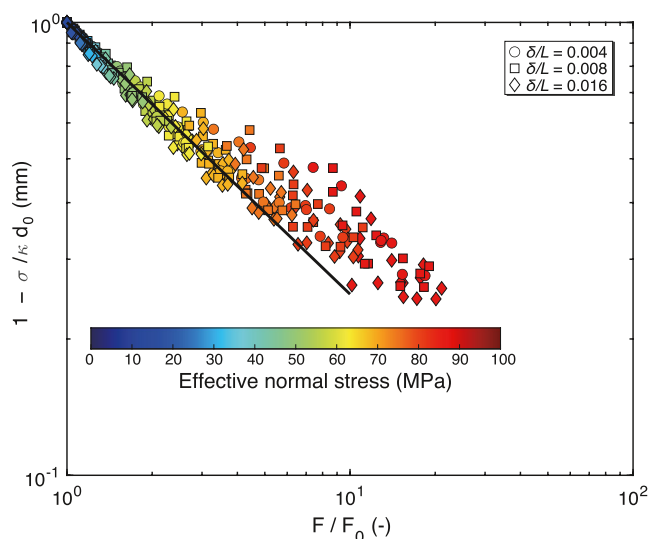
(11)

Figure 4. Correlation between fracture aperture changes and formation factor normalized to the values at $\sigma = 5$ MPa compiled from all data sets of faults. The colors and shapes of the symbols represent effective normal stress and shear displacement, respectively. The solid line denotes the prediction lines based on Equation 1.

where the subscript zero indicates an arbitrary reference value. Figure 4 plots the relationship between the normalized formation factor and stress-induced aperture closure based on our fault data sets considering the lowest stress condition. Overall, the relationship lies on a straight line ($m = 1.2$) independent of the fault size and its microstructures at $\sigma < \sim 70$ MPa (i.e., percolation threshold), demonstrating the validity of Equation 11 in the fully connected flow regime. This proposed formula of the electro-mechanical relationship implies that resistivity data possibly predict either stiffness or stress state. Given that crustal stress can be considered constant (i.e., on relatively short time scales), the observed changes in resistivity with changes in the effective normal stress represent changes in pore pressure. Note that a small fluctuation in the stress (shown in color in Figure 4) is due to the stress-dependent fracture specific stiffness, which varies with the roughness and size of the fault (Worthington, 2007). Importantly, the stress prediction line remains valid across various fracture data sets and additional 13,000 simulations conducted with varying random seeds (Figure S9 in Supporting Information S1). Given the in situ stiffness through a seismic survey (Hunziker et al., 2020; Minato & Ghose, 2016), Equation 11 can be used to predict the changes in pore pressure. In field measurements, a promising method to estimate in situ pore pressure is by applying the empirical fitting in terms of crack porosity reduction to seismic profiles (Kitajima & Saffer, 2012; Tonegawa et al., 2017; Tsuji et al., 2008, 2014). However, the commonly used effective medium theories for elasticity ignore the macroscopic fracture due to the noninteraction assumptions. The proposed formula using formation factor is preferable to estimate the changes in pore pressure associated with fault movements. Although further verification is required for practical application, we expect that this may provide new insights into estimating pore pressure in faulted regions using electrical resistivity monitoring.

5. Conclusions

This study investigated changes in permeability, resistivity, and their respective relationships at elevated normal stress by performing numerical simulations of various fracture models with varying fracture size, surface roughness, and shear displacement. Based on the deformed rough surfaces simulated using a half space–based dry contact model, we calculated the fracture flow using the lattice Boltzmann method and the electrical resistivity using the finite element method. The numerical results demonstrate that changes in fracture permeability and electrical resistivity at elevated normal stress are affected by fracture size, roughness, and shear displacement. Nevertheless, the relationships between permeability–resistivity exhibit less dependence on these geometric characteristics. The log–log plot of the permeability–resistivity shows inflection at the fracture permeability of approximately $10^{-11.5}$ m^2, and the microscopic flow analysis further supports that this inflection is related to the percolation of the dominant flow path. The trend of the relationship could be correlated with Archie's cementation exponent based on the equivalent channel model. These findings suggest that the permeability evolution of faults can be formulated with changes in resistivity regardless of the fracture size and its microstructures. In contrast, the resistivity–porosity relationship can vary depending on the tortuosity or connectivity, suggesting that the resistivity observation is less biased when directly estimating fracture permeability compared to porosity. In addition, an electro-mechanical relationship is proposed to estimate the changes in the stress state associated with fault movements. Although these proposed formulas are limited to single fractures and require further verification for practical application, they may provide new insights into electrical resistivity monitoring for estimating changes in permeability and pore pressure in fracture-dominated areas.

Data Availability Statement

All results are summarized in Supporting Information S1. The digital fracture data are available online from Digital Rocks Portal (Sawayama, 2023).

References

Ahrenholz, B., Tölke, J., Lehmann, P., Peters, A., Kaestner, A., Krafczyk, M., & Durner, W. (2008). Prediction of capillary hysteresis in a porous material using lattice-Boltzmann methods and comparison to experimental data and a morphological pore network model. *Advances in Water Resources*, *31*(9), 1151–1173. https://doi.org/10.1016/j.advwatres.2008.03.009

Aizawa, K., Kanda, W., Ogawa, Y., Iguchi, M., Yokoo, A., Yakiwara, H., & Sugano, T. (2011). Temporal changes in electrical resistivity at Sakurajima volcano from continuous magnetotelluric observations. *Journal of Volcanology and Geothermal Research*, *199*(1), 165–175. https://doi.org/10.1016/j.jvolgeores.2010.11.003

Anderson, R. N., Zoback, M. D., Hickman, S. H., & Newmark, R. L. (1985). Permeability versus depth in the upper oceanic crust: In situ measurements in DSDP hole 504B, eastern equatorial Pacific. *Journal of Geophysical Research*, *90*(B5), 3659–3669. https://doi.org/10.1029/jb090ib05p03659

Andrä, H., Combaret, N., Dvorkin, J., Glatt, E., Han, J., Kabel, M., et al. (2013). Digital rock physics benchmarks—Part II: Computing effective properties. *Computers & Geosciences*, *50*, 33–43. https://doi.org/10.1016/j.cageo.2012.09.008

Archie, G. E. (1942). The electrical resistivity log as an aid in determining some reservoir characteristics. *Transactions of the AIME*, *146*(01), 54–62. https://doi.org/10.2118/942054-g

Becker, K., Von Herzen, R. P., Francis, T. J. G., Anderson, R. N., Honnorez, J., Adamson, A. C., et al. (1982). In situ electrical resistivity and bulk porosity of the oceanic crust Costa Rica Rift. *Nature*, *300*(5893), 594–598. https://doi.org/10.1038/300594a0

Berkowitz, B. (1995). Analysis of fracture network connectivity using percolation theory. *Mathematical Geology*, *27*(4), 467–483. https://doi.org/10.1007/bf02084422

Bernabé, Y., Zamora, M., Li, M., Maineult, A., & Tang, Y. B. (2011). Pore connectivity, permeability, and electrical formation factor: A new model and comparison to experimental data. *Journal of Geophysical Research*, *116*(B11), B11204. https://doi.org/10.1029/2011jb008543

Brown, S. R. (1989). Transport of fluid and electric current through a single fracture. *Journal of Geophysical Research*, *94*(B7), 9429–9438. https://doi.org/10.1029/jb094ib07p09429

Brown, S. R. (1995). Simple mathematical model of a rough fracture. *Journal of Geophysical Research*, *100*(B4), 5941–5952. https://doi.org/10.1029/94jb03262

Brown, S. R., & Scholz, C. H. (1985). Broad bandwidth study of the topography of natural rock surfaces. *Journal of Geophysical Research*, *90*(B14), 12575–12582. https://doi.org/10.1029/jb090ib14p12575

Cai, J., Zhang, Z., Wei, W., Guo, D., Li, S., & Zhao, P. (2019). The critical factors for permeability-formation factor relation in reservoir rocks: Pore-throat ratio, tortuosity and connectivity. *Energy*, *188*, 116051. https://doi.org/10.1016/j.energy.2019.116051

Candela, T., & Brodsky, E. E. (2016). The minimum scale of grooving on faults. *Geology*, *44*(8), 603–606. https://doi.org/10.1130/g37934.1

Candela, T., Brodsky, E. E., Marone, C., & Elsworth, D. (2014). Laboratory evidence for particle mobilization as a mechanism for permeability enhancement via dynamic stressing. *Earth and Planetary Science Letters*, *392*, 279–291. https://doi.org/10.1016/j.epsl.2014.02.025

Candela, T., Brodsky, E. E., Marone, C., & Elsworth, D. (2015). Flow rate dictates permeability enhancement during fluid pressure oscillations in laboratory experiments. *Journal of Geophysical Research: Solid Earth*, *120*(4), 2037–2055. https://doi.org/10.1002/2014jb011511

Candela, T., Renard, F., Klinger, Y., Mair, K., Schmittbuhl, J., & Brodsky, E. E. (2012). Roughness of fault surfaces over nine decades of length scales. *Journal of Geophysical Research*, *117*(B8), B08409. https://doi.org/10.1029/2011jb009041

Chen, Y., Liang, W., Lian, H., Yang, J., & Nguyen, V. P. (2017). Experimental study on the effect of fracture geometric characteristics on the permeability in deformable rough-walled fractures. *International Journal of Rock Mechanics and Mining Sciences*, *98*, 121–140. https://doi.org/10.1016/j.ijrmms.2017.07.003

Chesley, C., Naif, S., Key, K., & Bassett, D. (2021). Fluid-rich subducting topography generates anomalous forearc porosity. *Nature*, *595*(7866), 255–260. https://doi.org/10.1038/s41586-021-03619-8

Colombier, M., Wadsworth, F. B., Gurioli, L., Scheu, B., Kueppers, U., Di Muro, A., & Dingwell, D. B. (2017). The evolution of pore connectivity in volcanic rocks. *Earth and Planetary Science Letters*, *462*, 99–109. https://doi.org/10.1016/j.epsl.2017.01.011

Didana, Y. L., Heinson, G., Thiel, S., & Krieger, L. (2017). Magnetotelluric monitoring of permeability enhancement at enhanced geothermal system project. *Geothermics*, *66*, 23–38. https://doi.org/10.1016/j.geothermics.2016.11.005

Durham, W. B., & Bonner, B. P. (1994). Self-propping and fluid flow in slightly offset joints at high effective pressures. *Journal of Geophysical Research*, *99*(B5), 9391–9399. https://doi.org/10.1029/94jb00242

Elkhoury, J. E., Brodsky, E. E., & Agnew, D. C. (2006). Seismic waves increase permeability. *Nature*, *441*(7097), 1135–1138. https://doi.org/10.1038/nature04798

Elkhoury, J. E., Niemeijer, A., Brodsky, E. E., & Marone, C. (2011). Laboratory observations of permeability enhancement by fluid pressure oscillation of in situ fractured rock. *Journal of Geophysical Research*, *116*(B2), 1–15. https://doi.org/10.1029/2010jb007759

Elsworth, D., Ishibashi, T., & Zhang, F. (2018). Permeability evolution and frictional stability of fabricated fractures with specified roughness. *Journal of Geophysical Research*, *123*(11), 9355–9375. https://doi.org/10.1029/2018JB016215

Garboczi, E. J. (1998). Finite element and finite difference programs for computing the linear electric and elastic properties of digital image of random materials. Natl. Inst. Stand. Technol. Interag. Rep. (p. 6269).

Ghanbarian, B., Hunt, A. G., Ewing, R. P., & Skinner, T. E. (2014). Universal scaling of the formation factor in porous media derived by combining percolation and effective medium theories. *Geophysical Research Letters*, *41*(11), 3884–3890. https://doi.org/10.1002/2014gl060180

Ghanbarian, B., & Male, F. (2021). Theoretical power-law relationship between permeability and formation factor. *Journal of Petroleum Science & Engineering*, *198*, 108249. https://doi.org/10.1016/j.petrol.2020.108249

Glover, P. W. (2009). What is the cementation exponent? A new interpretation. *The Leading Edge*, *28*(1), 82–85. https://doi.org/10.1190/1.3064150

Glover, P. W., Zadjali, I. I., & Frew, K. A. (2006). Permeability prediction from MICP and NMR data using an electrokinetic approach. *Geophysics*, *71*(4), F49–F60. https://doi.org/10.1190/1.2216930

Guéguen, Y., Chelidze, T., & Le Ravalec, M. (1997). Microstructures, percolation thresholds, and rock physical properties. *Tectonophysics*, *279*(1), 23–35. https://doi.org/10.1016/s0040-1951(97)00132-7

Gueguen, Y., & Dienes, J. (1989). Transport properties of rocks from statistics and percolation. *Mathematical Geology*, *21*(1), 1–13. https://doi.org/10.1007/bf00897237

Guéguen, Y., & Palciauskas, V. (1994). *Introduction to the physics of rocks*. Princeton University Press.

Hawkins, A. J., Becker, M. W., & Tester, J. W. (2018). Inert and adsorptive tracer tests for field measurement of flow-wetted surface area. *Water Resources Research*, *54*(8), 5341–5358. https://doi.org/10.1029/2017wr021910

Heuler, V. B., Inagaki, F., Morono, Y., Kubo, Y., & Maeda, L. (2017). Temperature limit of the deep bio-sphere off Muroto. In *Proceedings of the international ocean discovery program* (Vol. 370). International Ocean Discovery Program. https://doi.org/10.14379/iodp.proc.370.103.2017

Hilfer, R. (1992). Local-porosity theory for flow in porous media. *Physical Review B: Condensed Matter*, *45*(13), 7115–7121. https://doi.org/10.1103/physrevb.45.7115

Hirose, T., Hamada, Y., Tanikawa, W., Kamiya, N., Yamamoto, Y., Tsuji, T., et al. (2021). High fluid-pressure patches beneath the décollement: A potential source of slow earthquakes in the Nankai trough off cape Muroto. *Journal of Geophysical Research: Solid Earth*, *126*(6), e2021JB021831. https://doi.org/10.1029/2021jb021831

Hunt, A. G., & Sahimi, M. (2017). Flow, transport, and reaction in porous media: Percolation scaling, critical-path analysis, and effective medium approximation. *Reviews of Geophysics*, *55*(4), 993–1078. https://doi.org/10.1002/2017rg000558

Hunziker, J., Greenwood, A., Minato, S., Barbosa, N. D., Caspari, E., & Holliger, K. (2020). Bayesian full-waveform inversion of tube waves to estimate fracture aperture and compliance. *Solid Earth*, *11*(2), 657–668. https://doi.org/10.5194/se-11-657-2020

Ishibashi, T., Watanabe, N., Hirano, N., Okamoto, A., & Tsuchiya, N. (2015). Beyond-laboratory-scale prediction for channeling flows through subsurface rock fractures with heterogeneous aperture distributions revealed by laboratory evaluation. *Journal of Geophysical Research: Solid Earth*, *120*(1), 106–124. https://doi.org/10.1002/2014jb011555

Jiang, F., Tsuji, T., & Hu, C. (2014). Elucidating the role of interfacial tension for hydrological properties of two-phase flow in natural sandstone by an improved lattice Boltzmann method. *Transport in Porous Media*, *104*(1), 205–229. https://doi.org/10.1007/s11242-014-0329-0

Johnson, T. C., Burghardt, J., Strickland, C., Knox, H., Vermeul, V., White, M., et al. (2021). 4D proxy imaging of fracture dilation and stress shadowing using electrical resistivity tomography during high pressure injections into a dense rock formation. *Journal of Geophysical Research: Solid Earth*, *126*(11), e2021JB022298. https://doi.org/10.1029/2021jb022298

Katayama, I., Abe, N., Hatakeyama, K., Akamatsu, Y., Okazaki, K., Ulven, O. I., et al. (2020). Permeability profiles across the crust-mantle sections in the Oman drilling project inferred from dry and wet resistivity data. *Journal of Geophysical Research: Solid Earth*, *125*(8), e2019JB018698. https://doi.org/10.1029/2019jb018698

Katz, A. J., & Thompson, A. H. (1986). Quantitative prediction of permeability in porous rock. *Physical Review B: Condensed Matter*, *34*(11), 8179–8181. https://doi.org/10.1103/physrevb.34.8179

Kim, Y.-S., & Sanderson, D. J. (2005). The relationship between displacement and length of faults: A review. *Earth-Science Reviews*, *68*(3), 317–334. https://doi.org/10.1016/j.earscirev.2004.06.003

Kirkby, A., & Heinson, G. (2017). Three-dimensional resistor network modeling of the resistivity and permeability of fractured rocks. *Journal of Geophysical Research: Solid Earth*, *122*(4), 2653–2669. https://doi.org/10.1002/2016jb013854

Kirkby, A., Heinson, G., & Krieger, L. (2016). Relating permeability and electrical resistivity in fractures using random resistor network models. *Journal of Geophysical Research: Solid Earth*, *121*(3), 1546–1564. https://doi.org/10.1002/2015jb012541

Kitajima, H., & Saffer, D. M. (2012). Elevated pore pressure and anomalously low stress in regions of low frequency earthquakes along the Nankai Trough subduction megathrust. *Geophysical Research Letters*, *39*(23), L23301. https://doi.org/10.1029/2:012gl053793

Matsuki, K., Chida, Y., Sakaguchi, K., & Glover, P. W. J. (2006). Size effect on aperture and permeability of a fracture as estimated in large synthetic fractures. *International Journal of Rock Mechanics and Mining Sciences*, *43*(5), 726–755. https://doi.org/10.1016/j.ijrmms.2005.12.001

Mazzella, A., & Morrison, H. F. (1974). Electrical resistivity variations associated with earthquakes on the San Andreas fault. *Science*, *185*(4154), 855–857. https://doi.org/10.1126/science.185.4154.855

Minato, S., & Ghose, R. (2016). AVO inversion for a non-welded interface: Estimating compliances of a fluid-filled fracture. *Geophysical Journal International*, *206*(1), 56–62. https://doi.org/10.1093/gji/ggw138

Naif, S., Key, K., Constable, S., & Evans, R. L. (2016). Porosity and fluid budget of a water-rich megathrust revealed with electromagnetic data at the Middle America Trench. *Geochemistry, Geophysics, Geosystems*, *17*(11), 4495–4516. https://doi.org/10.1002/2016gc006556

Okoroafor, E. R., Co, C., & Horne, R. N. (2022). Numerical investigation of the impact of fracture aperture anisotropy on EGS thermal performance. *Geothermics*, *100*, 102354. https://doi.org/10.1016/j.geothermics.2022.102354

Park, S. K. (1991). Monitoring resistivity changes prior to earthquakes in Parkfield, California, with telluric arrays. *Journal of Geophysical Research: Solid Earth*, *96*(B9), 14211–14237. https://doi.org/10.1029/91jb01228

Paterson, M. S. (1983). The equivalent channel model for permeability and resistivity in fluid-saturated rock—A re-appraisal. *Mechanics of Materials*, *2*(4), 345–352. https://doi.org/10.1016/0167-6636(83)90025-x

Peacock, J. R., Thiel, S., Heinson, G. S., & Reid, P. (2013). Time-lapse magnetotelluric monitoring of an enhanced geothermal system. *Geophysics*, *78*(3), B121–B130. https://doi.org/10.1190/geo2012-0275.1

Peacock, J. R., Thiel, S., Reid, P., & Heinson, G. (2012). Magnetotelluric monitoring of a fluid injection: Example from an enhanced geothermal system. *Geophysical Research Letters*, *39*(18), 3–7. https://doi.org/10.1029/2012gl053080

Petrovitch, C. L., Pyrak-Nolte, L. J., & Nolte, D. D. (2014). Combined scaling of fluid flow and seismic stiffness in single fractures. *Rock Mechanics and Rock Engineering*, *47*(5), 1613–1623. https://doi.org/10.1007/s00603-014-0591-z

Polonsky, I. A., & Keer, L. M. (1999). A numerical method for solving rough contact problems based on the multi-level multi-summation and conjugate gradient techniques. *Wear: An International Journal on the Science and Technology of Friction Lubrication and Wear*, *231*(2), 206–219. https://doi.org/10.1016/s0043-1648(99)00113-1

Power, W. L., & Durham, W. B. (1997). Topography of natural and artificial fractures in granitic rocks: Implications for studies of rock friction and fluid migration. *International Journal of Rock Mechanics and Mining Sciences*, *34*(6), 979–989. https://doi.org/10.1016/s1365-1609(97)80007-x

Power, W. L., Tullis, T. E., Brown, S. R., Boitnott, G. N., & Scholz, C. H. (1987). Roughness of natural fault surfaces. *Geophysical Research Letters*, *14*(1), 29–32. https://doi.org/10.1029/gl014i001p00029

Pyrak-Nolte, L. J., Cook, N. G. W., & Nolte, D. D. (1988). Fluid percolation through single fractures. *Geophysical Research Letters*, *15*(11), 1247–1250. https://doi.org/10.1029/gl015i011p01247

Pyrak-Nolte, L. J., & Morris, J. P. (2000). Single fractures under normal stress: The relation between fracture specific stiffness and fluid flow. *International Journal of Rock Mechanics and Mining Sciences*, *37*(1), 245–262. https://doi.org/10.1016/s1365-1609(99)00104-5

Pyrak-Nolte, L. J., & Nolte, D. D. (2016). Approaching a universal scaling relationship between fracture stiffness and fluid flow. *Nature Communications*, *7*(1), 10663. https://doi.org/10.1038/ncomms10663

Renard, F., Candela, T., & Bouchaud, E. (2013). Constant dimensionality of fault roughness from the scale of micro-fractures to the scale of continents. *Geophysical Research Letters*, *40*(1), 83–87. https://doi.org/10.1029/2012GL054143

Revil, A., & Cathles, L. M., III. (1999). Permeability of shaly sands. *Water Resources Research*, *35*(3), 651–662. https://doi.org/10.1029/98wr02700

Revil, A., Kessouri, P., & Torres-Verdín, C. (2014). Electrical conductivity, induced polarization, and permeability of the Fontainebleau sandstone. *Geophysics*, *79*(5), D301–D318. https://doi.org/10.1190/geo2014-0036.1

Sawayama, K. (2023). 15 fractures of granite [Dataset]. Digital Rocks Portal. https://doi.org/10.17612/7ffv-c780

Sawayama, K., Ikeda, T., Tsuji, T., Jiang, F., Nishizawa, O., & Fujimitsu, Y. (2022). Elastic wave velocity changes due to the fracture aperture and density, and direct correlation with permeability: An energetic approach to mated rock fractures. *Journal of Geophysical Research: Solid Earth*, *127*(2), e2021JB022639. https://doi.org/10.1029/2021jb022639

Sawayama, K., Ishibashi, T., Jiang, F., Tsuji, T., & Fujimitsu, Y. (2021a). Relating hydraulic–electrical–elastic properties of natural rock fractures at elevated stress and associated transient changes of fracture flow. *Rock Mechanics and Rock Engineering*, *54*(5), 2145–2164. https://doi.org/10.1007/s00603-021-02391-5

Sawayama, K., Ishibashi, T., Jiang, F., Tsuji, T., Nishizawa, O., & Fujimitsu, Y. (2021b). Scale-independent relationship between permeability and resistivity in mated fractures with natural rough surfaces. *Geothermics*, *94*, 102065. https://doi.org/10.1016/j.geothermics.2021.102065

Sawayama, K., Kitamura, K., & Fujimitsu, Y. (2018). Laboratory measurements on electric and elastic properties of fractured geothermal reservoir rocks under simulated EGS conditions. *GRC Transactions*, *42*, 2459–2475.

Schlische, R. W., Young, S. S., Ackermann, R. V., & Gupta, A. (1996). Geometry and scaling relations of a population of very small rift-related normal faults. *Geology*, *24*(8), 683–686. https://doi.org/10.1130/0091-7613(1996)024<0683:gasroa>2.3.co;2

Schultz, R. A., Soliva, R., Fossen, H., Okubo, C. H., & Reeves, D. M. (2008). Dependence of displacement–length scaling relations for fractures and deformation bands on the volumetric changes across them. *Journal of Structural Geology*, *30*(11), 1405–1411. https://doi.org/10.1016/j.jsg.2008.08.001

Shi, Y., Liao, X., Zhang, D., & Liu, C.-P. (2019). Seismic waves could decrease the permeability of the shallow crust. *Geophysical Research Letters*, *46*(12), 6371–6377. https://doi.org/10.1029/2019gl081974

Shi, Z., Zhang, S., Yan, R., & Wang, G. (2018). Fault zone permeability decrease following large earthquakes in a hydrothermal system. *Geophysical Research Letters*, *45*(3), 1387–1394. https://doi.org/10.1002/2017gl075821

Shokouhi, P., Jin, J., Wood, C., Rivière, J., Madara, B., Elsworth, D., & Marone, C. (2020). Dynamic stressing of naturally fractured rocks: On the relation between transient changes in permeability and elastic wave velocity. *Geophysical Research Letters*, *47*(1), 1–10. https://doi.org/10.1029/2019gl083557

Sibson, R. H. (1987). Earthquake rupturing as a mineralizing agent in hydrothermal systems. *Geology*, *15*(8), 701–704. https://doi.org/10.1130/0091-7613(1987)15<701:eraama>2.0.co;2

Slagle, A. L., & Goldberg, D. S. (2011). Evaluation of ocean crustal Sites 1256 and 504 for long-term CO_2 sequestration. *Geophysical Research Letters*, *38*(16), L16307. https://doi.org/10.1029/2011gl048613

Stesky, R. M. (1986). Electrical conductivity of brine-saturated fractured rock. *Geophysics*, *51*(8), 1585–1593. https://doi.org/10.1190/1.1442209

Sun, X., Xiang, Y., & Shi, Z. (2019). Changes in permeability caused by two consecutive earthquakes—Insights from the responses of a well-aquifer system to seismic waves. *Geophysical Research Letters*, *46*(17–18), 10367–10374. https://doi.org/10.1029/2019gl084704

Tonegawa, T., Araki, E., Kimura, T., Nakamura, T., Nakano, M., & Suzuki, K. (2017). Sporadic low-velocity volumes spatially correlate with shallow very low frequency earthquake clusters. *Nature Communications*, *8*(1), 2048. https://doi.org/10.1038/s41467-017-02276-8

Tsang, Y. W., & Witherspoon, P. A. (1981). Hydromechanical behavior of a deformable rock fracture subject to normal stress. *Journal of Geophysical Research*, *86*(B10), 9287–9298. https://doi.org/10.1029/jb086ib10p09287

Tsuji, T., Kamei, R., & Pratt, R. G. (2014). Pore pressure distribution of a mega-splay fault system in the Nankai Trough subduction zone: Insight into up-dip extent of the seismogenic zone. *Earth and Planetary Science Letters*, *396*, 165–178. https://doi.org/10.1016/j.epsl.2014.04.011

Tsuji, T., Tokuyama, H., Costa Pisani, P., & Moore, G. (2008). Effective stress and pore pressure in the Nankai accretionary prism off the Muroto Peninsula, southwestern Japan. *Journal of Geophysical Research*, *113*(B11), B11401. https://doi.org/10.1029/2007jb005002

Vogler, D., Settgast, R. R., Annavarapu, C., Madonna, C., Bayer, P., & Amann, F. (2018). Experiments and simulations of fully hydro-mechanically coupled response of rough fractures exposed to high-pressure fluid injection. *Journal of Geophysical Research: Solid Earth*, *123*(2), 1186–1200. https://doi.org/10.1002/2017jb015057

Walsh, J. B., & Brace, W. F. (1984). The effect of pressure on porosity and the transport properties of rock. *Journal of Geophysical Research*, *89*(B11), 9425–9431. https://doi.org/10.1029/jb089ib11p09425

Walsh, R., McDermott, C., & Kolditz, O. (2008). Numerical modeling of stress-permeability coupling in rough fractures. *Hydrogeology Journal*, *16*(4), 613–627. https://doi.org/10.1007/s10040-007-0254-1

Wang, L., & Cardenas, M. B. (2016). Development of an empirical model relating permeability and specific stiffness for rough fractures from numerical deformation experiments. *Journal of Geophysical Research: Solid Earth*, *121*(7), 4977–4989. https://doi.org/10.1002/2016jb013004

Watanabe, N., Hirano, N., & Tsuchiya, N. (2008). Determination of aperture structure and fluid flow in a rock fracture by high-resolution numerical modeling on the basis of a flow-through experiment under confining pressure. *Water Resources Research*, *44*(6), 1–11. https://doi.org/10.1029/2006wr005411

Witherspoon, P. A., Wang, J. S. Y., Iwai, K., & Gale, J. E. (1980). Validity of cubic law for fluid flow in a deformable rock fracture. *Water Resources Research*, *16*(6), 1016–1024. https://doi.org/10.1029/wr016i006p01016

Wood, C. E., Shokouhi, P., Manogharan, P., Rivère, J., Elsworth, D., & Marone, C. (2021). Imaging elastodynamic and hydraulic properties of in situ fractured rock: An experimental investigation exploring effects of dynamic stressing and shearing. *Journal of Geophysical Research: Solid Earth*, *126*(11), e2020JB021521. https://doi.org/10.1029/2020jb021521

Worthington, M. (2007). The compliance of macrofractures. *The Leading Edge*, *26*(9), 1118–1122. https://doi.org/10.1190/1.2780780

Wu, J., Goto, T.-N., & Koike, K. (2021). Estimating fractured rock effective permeability using discrete fracture networks constrained by electrical resistivity data. *Engineering Geology*, *289*, 106178. https://doi.org/10.1016/j.enggeo.2021.106178

Xue, L., Li, H.-B., Brodsky, E. E., Xu, Z.-Q., Kano, Y., Wang, H., et al. (2013). Continuous permeability measurements record healing inside the Wenchuan earthquake fault zone. *Science*, *340*(6140), 1555–1559. https://doi.org/10.1126/science.1237237

Yamaya, Y., Suzuki, Y., Murata, Y., Okamoto, K., Watanabe, N., Asanuma, H., et al. (2022). 3-D resistivity imaging of the supercritical geothermal system in the Sengan geothermal region, NE Japan. *Geothermics*, *103*, 102412. https://doi.org/10.1016/j.geothermics.2022.102412

Zimmerman, R. W., Chen, D.-W., & Cook, N. G. W. (1992). The effect of contact area on the permeability of fractures. *Journal of Hydrology*, *139*(1), 79–96. https://doi.org/10.1016/0022-1694(92)90196-3

References From the Supporting Information

Chen, Z., Narayan, S. P., Yang, Z., & Rahman, S. S. (2000). An experimental investigation of hydraulic behavior of fractures and joints in granitic rock. *International Journal of Rock Mechanics and Mining Sciences*, *37*(7), 1061–1071. https://doi.org/10.1016/s1365-1609(00)00039-3

Ishibashi, T., Watanabe, N., Asanuma, H., & Tsuchiya, N. (2016). Linking microearthquakes to fracture permeability change: The role of surface roughness. *Geophysical Research Letters*, *43*(14), 7486–7493. https://doi.org/10.1002/2016gl069478

京都大学
KYOTO UNIVERSITY

A Self-archived copy in
Kyoto University Research Information Repository
https://repository.kulib.kyoto-u.ac.jp

京都大学学術情報リポジトリ
KURENAI 紅
Kyoto University Research Information Repository

Johnson, K. L., Greenwood, J. A., & Higginson, J. G. (1985). The contact of elastic regular wavy surfaces. *International Journal of Mechanical Sciences*, *27*(6), 383–396. https://doi.org/10.1016/0020-7403(85)90029-3

Kanamori, H., & Anderson, D. L. (1975). Theoretical basis of some empirical relations in seismology. *Bulletin of the Seismological Society of America*, *65*, 1073–1095.

Mallikamas, W., & Rajaram, H. (2005). On the anisotropy of the aperture correlation and effective transmissivity in fractures generated by sliding between identical self-affine surfaces. *Geophysical Research Letters*, *32*(11), L11401. https://doi.org/10.1029/2005gl022859